NMR Structure of the Bank Vole Prion Protein at 20 °C Contains a Structured Loop of Residues 165–171

Christen, Barbara ; Perez, Daniel Raoul ; Hornemann, Simone ; Wüthrich, Kurt

Abstract: The recent introduction of bank vole (Clethrionomys glareolus) as an additional laboratory animal for research on prion diseases revealed an important difference when compared to the mouse and the Syrian hamster, since bank voles show a high susceptibility to infection by brain homogenates from a wide range of diseased species such as sheep, goats, and humans. In this context, we determined the NMR structure of the C-terminal globular domain of the recombinant bank vole prion protein (bvPrP) [bvPrP(121–231)] at 20 °C. bvPrP(121–231) has the same overall architecture as other mammalian PrPs, with three -helices and an antiparallel -sheet, but it differs from PrP of the mouse and most other mammalian species in that the loop connecting the second -strand and helix 2 is precisely defined at 20 °C. This is similar to the previously described structures of elk PrP and the designed mouse PrP (mPrP) variant mPrP[S170N,N174T](121–231), whereas Syrian hamster PrP displays a structure that is in-between these limiting cases. Studies with the newly designed variant mPrP[S170N](121–231), which contains the same loop sequence as bvPrP, now also showed that the single-amino-acid substitution S170N in mPrP is sufficient for obtaining a well-defined loop, thus providing the rationale for this local structural feature in bvPrP.

DOI: https://doi.org/10.1016/j.jmb.2008.08.045

NMR Structure of the Bank Vole Prion Protein at 20°C Contains a Structured Loop of Residues 165–171

Barbara Christen, Daniel R. Pérez, Simone Hornemann, and Kurt Wüthrich*

Institute of Molecular Biology and Biophysics, ETH Zurich, CH-8093 Zurich, Switzerland

Running title: Bank Vole Prion Protein Structure

*Corresponding author:

Kurt Wüthrich

Institute of Molecular Biology and Biophysics

Schafmattstrasse 20

ETH Zurich

CH-8093 Zurich, Switzerland

telephone: +41 44 633 24 73

fax: +41 44 633 11 51

e-mail: wuthrich@mol.biol.ethz.ch

www.mol.biol.ethz.ch/groups/wuthrich_group

Character count (including spaces): 32225

Abbreviations: PrP, prion protein; bvPrP, bank vole PrP; ePrP, elk PrP; HSQC, heteronuclear single quantum coherence; mPrP, mouse PrP; mPrP[S170N](121–231), polypeptide segment of residues 121–231 of the variant of mPrP with Ser170 replaced by Asn (see Schätzl *et al.*[45] for the numeration used); NOE, nuclear Overhauser enhancement; NOESY, nuclear Overhauser enhancement spectroscopy; shPrP, Syrian hamster PrP; TOCSY, total correlation spectroscopy; TSE, transmissible spongiform encephalopathy.

Keywords: bank vole; prion protein; NMR structure; transmissible spongiform encephalopathies; species barrier.

Abstract

The recent introduction of the bank vole (*Clethrionomys glareolus*) as an additional laboratory animal for research on prion diseases revealed an important difference when compared to the mouse and the Syrian hamster, since bank voles show high susceptibility to infection by brain homogenate from a wide range of diseased species, such as sheep, goat and man. In this context, we determined the NMR structure of the C-terminal globular domain of the recombinant bank vole prion protein (bvPrP(121–231)) at 20°C. bvPrP(121–231) has the same overall architecture as other mammalian PrPs, with three α-helices and an antiparallel β-sheet, but it differs from PrP of the mouse and most other mammalian species in that the loop connecting the second β-strand and the helix α2 is precisely defined at 20°C. This is similar to the previously described structures of elk PrP and the designed mouse PrP variant mPrP[S170N,N174T](121–231), whereas Syrian hamster PrP displays a structure that is in-between these limiting cases. Studies with the newly designed variant mPrP[S170N](121–231), which contains the same loop sequence as bvPrP, now also showed that the single-amino acid substitution S170N in mouse PrP is sufficient for obtaining a well-defined loop, thus providing the rationale for this local structural feature in bvPrP.

Introduction

The bank vole (*Clethrionomys glareolus*) has recently attracted interest due to unexpected features revealed by its use as a new laboratory animal for the investigation of prion diseases. When compared to the mouse and the Syrian hamster, bank voles are highly susceptible to infection by sheep and goat scrapie, and various human strains of transmissible spongiform encephalopathies (TSE) also show a low transmission barrier.[1-3] Responding to the ensuing interest in the three-dimensional structure of bank vole PrP (bvPrP), this paper describes the NMR structure of the C-terminal globular domain in the healthy, cellular form of bvPrP ($bvPrP^C$) at 20°C. To support the analysis of the structure of bvPrP(121–231), we further solved the structure of a designed mouse PrP (mPrP) variant, mPrP[S170N](121–231), and pursued a detailed comparison of the two structures.

Prion diseases, or TSEs, are a group of neurodegenerative diseases which include scrapie in sheep, Creutzfeldt-Jakob disease (CJD) in humans, bovine spongiform encephalopathy (BSE) in cattle, and chronic wasting disease (CWD) in mule deer and elk.[4-6] Critical events in the development and propagation of TSEs include the conversion of the cellular prion protein, PrP^C, to a protease-resistant aggregated isoform, PrP^{Sc}, which accumulates most pronouncedly in neurologic tissues of the affected organisms.[4] While TSEs can be transmitted within the same species, “transmission barriers” make interspecies transmission inefficient, as evidenced either by complete absence of detectable transmission or by prolonged incubation periods prior to onset of clinical signs.[7] The occurrence of “new variant CJD” in humans in the 1990s, which was attributed to the prion strain identified in BSE-infected cattle in the 1980s,[8-11] emphasized the critical importance of transmission barriers and the possibility of their breakdown for food management and for public health services.

The amino acid sequence homology between PrP of the host and the donor is the basic determinant of the barrier between different species,[7] whereby single-amino acid exchanges can cause a significant change in the susceptibility to infection.[7,12] It has also been argued that the efficiency of transmission could further be affected by variation of the PrP^C conformations of the donor and the recipient.[13] The three-dimensional structures of PrP^C from various species have been solved by solution NMR, including humans, cattle, sheep and elk, and the widely used laboratory animals hamster and mouse.[14-21] The global PrP^C architecture in all mammalian species studied so far is nearly identical, with a flexibly extended 100-residue N-terminal tail and a 100-residue globular C-terminal domain, which contains three α-helices and an antiparallel β-sheet. Nonetheless, subtle local structure variations between different species were observed in the globular domain, in particular in a loop formed by the residues 165–171, which link the second β-strand and the helix α2. At 20°C, the β2–α2 loop is precisely defined in PrP^C from elk PrP ($ePrP^C$), but disordered in the NMR structures of PrP^C from a variety of other species, including man, cattle, sheep and mouse, and is partially ordered in PrP^C from Syrian hamster ($shPrP^C$) at 30°C. This special structural feature in ePrP(121–231) was attributed to the nature of the amino acid residues in positions 170 and 174, since the three-dimensional structure of the designed mouse variant mPrP[S170N,N174T](121–231) also includes a precisely structured loop of residues 165–171 at 20°C.[20]

Cloning, expression and purification of bvPrP(121–231) and mPrP[S170N](121–231)

The amino acid sequence of bvPrP(121–231) differs from mPrP(121–231) at only four positions (Figure 1). Therefore we used site-directed mutagenesis to replace these four residues in mPrP(121–231) in order to obtain the gene encoding bvPrP^{C}. Similarly, we used site-directed mutagenesis with mPrP(121–231) to generate mPrP[S170N](121–231). For the NMR structure determinations of bvPrP(121–231) and mPrP[S170N](121–231), the uniformly ^{15}N- and ^{13}C,^{15}N-labeled proteins were produced in *Escherichia coli* and purified using the standard protocol for mammalian PrP^{C}s.[17,22]

NMR structure determination of bvPrP(121–231) and mPrP[S170N](121–231)

Nearly complete sequence-specific backbone and amino acid side chain assignments were obtained for bvPrP(121–231) and mPrP[S170N](121–231), including all of the residues 167–171 and 175, which were not observed in mPrP(121–231)[14], with H^{α} of Phe175 being the only missing backbone assignment in bvPrP(121–231). Steady-state $^{15}N\{^{1}H\}$-heteronuclear NOE data then indicated that bvPrP(121–231) and mPrP[S170N](121–231) form a globular domain, with positive NOE-values near 0.8 for the residues 125–228, and that the flanking residues 121–124 and 229–231 undergo high-frequency motions, as evidenced by negative $^{15}N\{^{1}H\}$-NOE values (data not shown).

On the basis of the essentially complete resonance assignments, a high-quality structure determination for the globular domain was obtained, as documented by the statistics for the final ATNOS/CANDID/DYANA cycle of the structure determination (Table 1) and the displays of the structure in Figure 2. The figure 2A shows that bvPrP(121–231) contains three α-helices spanning the residues 144–156, 172–194 and 200–225, and a two-stranded antiparallel β-sheet of residues 128–131 and 161–164. The helices α1 and α2 end with a 3_{10}-helical turn, and a 3_{10}-helical turn is also formed by the residues 165–169. The side-chains are well-defined, with the ones in the hydrophobic core bounded by the helices α2 and α3 having mean global displacements of less than 0.6 Å (Figure 2B).

The structure determination of mPrP[S170N](121–231) converged with closely similar statistics as bvPrP(121–231) (Table 1). The two structures can be superimposed with an rmsd value of 1.5 Å for the backbone heavy atoms. A superposition of the two structures (Figure 3C) visualizes the near-identity of the two folds, where the C-terminal end of helix α2 is less precisely defined in mPrP[S170N](121–231).

Local structure variations in the globular domains of bvPrP(121–231), mPrP(121–231) and mPrP[S170N](121–231) and possible correlations with TSE transmission

Earlier experiments with bank vole PrP provided indications that the residues in positions 155 and 170 have an important role for the conversion of bvPrP^{C} into bvPrP^{Sc}.[2,3] Both positions show high variation among mammalian species.[23,24] In the three-dimensional structure they are both solvent-exposed, and they are located in two well separated molecular regions that have previously been discussed as important structural epitopes for TSE transmission,[14] including that the helix α1 in PrP^{C} has been suggested to act as an initiation site for the structural conversion.[25] The transmission barrier between mouse PrP^{C} and Syrian hamster PrP^{Sc} was actually traced back to residue 155 in the helix α1.[26] Superpositions of the three-dimensional NMR structure of bvPrP(121–231) with mPrP(121–231) (Figure 3A), shPrP(121–231) (Figure 3B) and the designed variant protein mPrP[S170N](121–231) (Figure 3C) now show that there is no significant structural variation near to the helix α1 among these three species. Therefore, it seems likely that the chemical nature of the amino acid residue in position 155 contributes to the higher TSE susceptibility of bank voles, rather than its impact on the local three-dimensional structure.

The residue 170 is located in a surface epitope formed by the β2–α2 loop and parts of the helix α3. This epitope was previously suggested to be a recognition site in a mouse/human chimera PrP^{C} for a potential chaperone, designated as “protein X”, which would promote the conversion of PrP^{C} into PrP^{Sc}.[27,28] Figure 3 shows that the β2–α2 loop is precisely defined for both bvPrP(121–231) and mPrP[S170N](121–231) at 20°C, as was previously also observed for ePrP(121–231) and mPrP[S170N,N174T](121–231),[20] and that it is also quite well defined in shPrP(121–231) at 30°C.[15] All the backbone amide

resonances of the loop residues are present in the 2D [^{15}N,^{1}H]-HSQC spectra of Figure 4, B and C, whereas they are absent in the spectrum of Figure 4A, which is the reason why the NMR structure of mPrP(121–231) contains a disordered β2–α2 loop.[14,20] One notices further that the C-terminal end of helix α3 forms closer contacts with the β2–α2 loop in bvPrP(121–231), mPrP[S170N](121–231) and shPrP(121–231) than in mPrP(121–231) (Figure 3). A close approach of the helix α3 to the β2–α2 loop was also observed in ePrP(121–231) and mPrP[S170N,N174T](121–231).[20]

Molecular dynamics calculations with the cellular form of the mouse prion protein[29] provide support for the experimental observation that the residue Ser170 has a marked influence on the conformational properties of the β2–α2 loop in mPrP^{C}.

Finally, it is striking that both bank voles and cervids carry an asparagine residue at position 170, which seems to be correlated either with a higher susceptibility to horizontal TSE transmission[30], or a lower transmission barrier to inter-species transmission.[31] The impact of the nature of the residue 170 on the conformation of the β2–α2 loop in PrP^{C} thus appears to propagate to species-specific intermolecular contacts. In this way the loop conformation could assume a trigger function in the disease-related conversion of PrP^{C} into PrP^{Sc}. To further investigate possible physiological consequences of structural variations in the β2–α2 loop, studies with transgenic mice expressing PrP[S170N,N174T], which corresponds to the β2–α2 loop sequence of ePrP,[20] are pursued in a collaboration with the group of A. Aguzzi at the University of Zürich.

Data bank accession codes

The atomic coordinates for bvPrP(121–231) and mPrP[S170N](121–231) have been deposited in the Protein Data Bank (www.pdb.org, PDB ID codes 2k56 and 2k5o); the chemical shift lists are available at the BioMagResBank (www.bmrb.wisc.edu, accession numbers 15824 and 15845).

Acknowledgements

We thank Dr. Fred F. Damberger for helpful discussions. Financial support by the Swiss National Science Foundation and the Federal Institute of Technology Zürich through the National Center of Competence in Research (NCCR) “Structural Biology” and by the European Union (UPMAN, project number 512052) is gratefully acknowledged.

References

1. Nonno, R., Di Bari, M. A., Cardone, F., Vaccari, G., Fazzi, P., Dell'Omo, G., Cartoni, C., Ingrosso, L., Boyle, A., Galeno, R., Sbriccoli, M., Lipp, H. P., Bruce, M., Pocchiari, M. & Agrimi, U. (2006). Efficient transmission and characterization of Creutzfeldt-Jakob disease strains in bank voles. *PLoS Pathog* **2**, e12.
2. Piening, N., Nonno, R., Di Bari, M., Walter, S., Windl, O., Agrimi, U., Kretzschmar, H. A. & Bertsch, U. (2006). Conversion efficiency of bank vole prion protein in vitro is determined by residues 155 and 170, but does not correlate with the high susceptibility of bank voles to sheep scrapie in vivo. *J Biol Chem* **281**, 9373–9384.
3. Agrimi, U., Nonno, R., Dell'Omo, G., Di Bari, M. A., Conte, M., Chiappini, B., Esposito, E., Di Guardo, G., Windl, O., Vaccari, G. & Lipp, H. P. (2008). Prion protein amino acid determinants of differential susceptibility and molecular feature of prion strains in mice and voles. *PLoS Pathog* **4**, e1000113.
4. Prusiner, S. B. (1998). Prions. *Proc Natl Acad Sci USA* **95**, 13363–13383.
5. Collinge, J. (2001). Prion diseases of humans and animals: their causes and molecular basis. *Annu Rev Neurosci* **24**, 519–550.
6. Weissmann, C., Enari, M., Klohn, P. C., Rossi, D. & Flechsig, E. (2002). Transmission of prions. *Proc Natl Acad Sci USA* **99**, 16378–16383.
7. Moore, R. A., Vorberg, I. & Priola, S. A. (2005). Species barriers in prion diseases – brief review. *Arch Virol* **Suppl 19**, 187–202.
8. Collinge, J., Sidle, K. C., Meads, J., Ironside, J. & Hill, A. F. (1996). Molecular analysis of prion strain variation and the aetiology of 'new variant' CJD. *Nature* **383**, 685–690.
9. Bruce, M. E., Will, R. G., Ironside, J. W., McConnell, I., Drummond, D., Suttie, A., McCardle, L., Chree, A., Hope, J., Birkett, C., Cousens, S., Fraser, H. & Bostock, C.

J. (1997). Transmissions to mice indicate that 'new variant' CJD is caused by the BSE agent. *Nature* **389**, 498–501.

10. Hill, A. F., Desbruslais, M., Joiner, S., Sidle, K. C., Gowland, I., Collinge, J., Doey, L. J. & Lantos, P. (1997). The same prion strain causes vCJD and BSE. *Nature* **389**, 448–450, 526.
11. Collinge, J. (1999). Variant Creutzfeldt-Jakob disease. *Lancet* **354**, 317–323.
12. Westaway, D., Goodman, P. A., Mirenda, C. A., McKinley, M. P., Carlson, G. A. & Prusiner, S. B. (1987). Distinct prion proteins in short and long scrapie incubation period mice. *Cell* **51**, 651–662.
13. Hill, A. F. & Collinge, J. (2002). Species-barrier-independent prion replication in apparently resistant species. *Apmis* **110**, 44–53.
14. Riek, R., Hornemann, S., Wider, G., Billeter, M., Glockshuber, R. & Wüthrich, K. (1996). NMR structure of the mouse prion protein domain PrP(121–231). *Nature* **382**, 180–182.
15. James, T. L., Liu, H., Ulyanov, N. B., Farr-Jones, S., Zhang, H., Donne, D. G., Kaneko, K., Groth, D., Mehlhorn, I., Prusiner, S. B. & Cohen, F. E. (1997). Solution structure of a 142-residue recombinant prion protein corresponding to the infectious fragment of the scrapie isoform. *Proc Natl Acad Sci USA* **94**, 10086–10091.
16. Liu, H., Farr-Jones, S., Ulyanov, N. B., Llinas, M., Marqusee, S., Groth, D., Cohen, F. E., Prusiner, S. B. & James, T. L. (1999). Solution structure of Syrian hamster prion protein rPrP(90–231). *Biochemistry* **38**, 5362–5377.
17. Zahn, R., Liu, A., Lührs, T., Riek, R., von Schroetter, C., López-García, F., Billeter, M., Calzolai, L., Wider, G. & Wüthrich, K. (2000). NMR solution structure of the human prion protein. *Proc Natl Acad Sci USA* **97**, 145–150.

18. López-García, F., Zahn, R., Riek, R. & Wüthrich, K. (2000). NMR structure of the bovine prion protein. *Proc Natl Acad Sci USA* **97**, 8334–8339.
19. Hornemann, S., Schorn, C. & Wüthrich, K. (2004). NMR structure of the bovine prion protein isolated from healthy calf brains. *EMBO Rep* **5**, 1159–1164.
20. Gossert, A. D., Bonjour, S., Lysek, D. A., Fiorito, F. & Wüthrich, K. (2005). Prion protein NMR structures of elk and of mouse/elk hybrids. *Proc Natl Acad Sci USA* **102**, 646–650.
21. Lysek, D. A., Schorn, C., Nivon, L. G., Esteve-Moya, V., Christen, B., Calzolai, L., von Schroetter, C., Fiorito, F., Herrmann, T., Güntert, P. & Wüthrich, K. (2005). Prion protein NMR structures of cats, dogs, pigs, and sheep. *Proc Natl Acad Sci USA* **102**, 640–645.
22. Lysek, D. A. & Wüthrich, K. (2004). Prion protein interaction with the C-terminal SH3 domain of Grb2 studied using NMR and optical spectroscopy. *Biochemistry* **43**, 10393–10399.
23. Wopfner, F., Weidenhofer, G., Schneider, R., von Brunn, A., Gilch, S., Schwarz, T. F., Werner, T. & Schätzl, H. M. (1999). Analysis of 27 mammalian and 9 avian PrPs reveals high conservation of flexible regions of the prion protein. *J Mol Biol* **289**, 1163–1178.
24. van Rheede, T., Smolenaars, M. M., Madsen, O. & de Jong, W. W. (2003). Molecular evolution of the mammalian prion protein. *Mol Biol Evol* **20**, 111–121.
25. Morrissey, M. P. & Shakhnovich, E. I. (1999). Evidence for the role of PrP^C helix 1 in the hydrophilic seeding of prion aggregates. *Proc Natl Acad Sci USA* **96**, 11293–11298.

26. Priola, S. A., Chabry, J. & Chan, K. (2001). Efficient conversion of normal prion protein (PrP) by abnormal hamster PrP is determined by homology at amino acid residue 155. *J Virol* **75**, 4673–4680.

27. Telling, G. C., Scott, M., Mastrianni, J., Gabizon, R., Torchia, M., Cohen, F. E., DeArmond, S. J. & Prusiner, S. B. (1995). Prion propagation in mice expressing human and chimeric PrP transgenes implicates the interaction of cellular PrP with another protein. *Cell* **83**, 79–90.

28. Kaneko, K., Zulianello, L., Scott, M., Cooper, C. M., Wallace, A. C., James, T. L., Cohen, F. E. & Prusiner, S. B. (1997). Evidence for protein X binding to a discontinuous epitope on the cellular prion protein during scrapie prion propagation. *Proc Natl Acad Sci USA* **94**, 10069–10074.

29. Gorfe, A. A. & Caflisch, A. (2007). Ser170 controls the conformational multiplicity of the loop 166–175 in prion proteins: implication for conversion and species barrier. *Faseb J* **21**, 3279–3287.

30. Sigurdson, C. J. & Aguzzi, A. (2007). Chronic wasting disease. *Biochim Biophys Acta* **1772**, 610–618.

31. Cartoni, C., Schinina, M. E., Maras, B., Nonno, R., Vaccari, G., Di Baria, M. A., Conte, M., Liu, Q. G., Lu, M., Cardone, F., Windl, O., Pocchiari, M. & Agrimi, U. (2005). Identification of the pathological prion protein allotypes in scrapie-infected heterozygous bank voles (*Clethrionomys glareolus*) by high-performance liquid chromatography-mass spectrometry. *J Chromatogr A* **1081**, 122–126.

32. Billeter, M., Kline, A. D., Braun, W., Huber, R. & Wüthrich, K. (1989). Comparison of the high-resolution structures of the alpha-amylase inhibitor tendamistat determined

by nuclear magnetic resonance in solution and by X-ray diffraction in single crystals. *J Mol Biol* **206**, 677–687.

33. Bax, A. & Grzesiek, S. (1993). Methodological advances in protein NMR. *Acc Chem Res* **26**, 131–138.
34. Dayie, K. T. & Wagner, G. (1994). Relaxation-rate measurements for 15N-1H groups with pulsed-field gradients and preservation of coherence pathways. *J Magn Reson A* **111**, 121–126.
35. Renner, C., Schleicher, M., Moroder, L. & Holak, T. A. (2002). Practical aspects of the 2D ^{15}N-{^{1}H}-NOE experiment. *J Biomol NMR* **23**, 23–33.
36. Keller, R. (2004). *The Computer-aided Resonance Assignment Tutorial CARA*. Cantina Verlag, Goldau, Switzerland.
37. Herrmann, T., Güntert, P. & Wüthrich, K. (2002). Protein NMR structure determination with automated NOE-identification in the NOESY spectra using the new software ATNOS. *J Biomol NMR* **24**, 171–189.
38. Herrmann, T., Güntert, P. & Wüthrich, K. (2002). Protein NMR structure determination with automated NOE assignment using the new software CANDID and the torsion angle dynamics algorithm DYANA. *J Mol Biol* **319**, 209–227.
39. Güntert, P., Mumenthaler, C. & Wüthrich, K. (1997). Torsion angle dynamics for NMR structure calculation with the new program DYANA. *J Mol Biol* **273**, 283–298.
40. Luginbühl, P., Güntert, P., Billeter, M. & Wüthrich, K. (1996). The new program OPAL for molecular dynamics simulations and energy refinements of biological macromolecules. *J Biomol NMR* **8**, 136–146.
41. Cornell, W. D., Cieplak, P., Bayly, C. I., Gould, I. R., Merz, K. M., Jr., Ferguson, D. M., Spellmeyer, D. C., Fox, T., Caldwell, J. W. & Kollman, P. A. (1995). A second

generation force field for the simulation of proteins, nucleic acids, and organic molecules. *J Am Chem Soc* **117**, 5179–5197.

42. Koradi, R., Billeter, M. & Wüthrich, K. (1996). MOLMOL: a program for display and analysis of macromolecular structures. *J Mol Graph* **14**, 51–55.
43. Kabsch, W. & Sander, C. (1983). Dictionary of protein secondary structure: pattern recognition of hydrogen-bonded and geometrical features. *Biopolymers* **22**, 2577–2637.
44. Morris, A. L., MacArthur, M. W., Hutchinson, E. G. & Thornton, J. M. (1992). Stereochemical quality of protein structure coordinates. *Proteins* **12**, 345–364.
1. Nonno, R., Di Bari, M. A., Cardone, F., Vaccari, G., Fazzi, P., Dell'Omo, G., Cartoni, C., Ingrosso, L., Boyle, A., Galeno, R., Sbriccoli, M., Lipp, H. P., Bruce, M., Pocchiari, M. & Agrimi, U. (2006). Efficient transmission and characterization of Creutzfeldt-Jakob disease strains in bank voles. *PLoS Pathog* **2**, e12.
2. Piening, N., Nonno, R., Di Bari, M., Walter, S., Windl, O., Agrimi, U., Kretzschmar, H. A. & Bertsch, U. (2006). Conversion efficiency of bank vole prion protein in vitro is determined by residues 155 and 170, but does not correlate with the high susceptibility of bank voles to sheep scrapie in vivo. *J Biol Chem* **281**, 9373–9384.
3. Agrimi, U., Nonno, R., Dell'Omo, G., Di Bari, M. A., Conte, M., Chiappini, B., Esposito, E., Di Guardo, G., Windl, O., Vaccari, G. & Lipp, H. P. (2008). Prion protein amino acid determinants of differential susceptibility and molecular feature of prion strains in mice and voles. *PLoS Pathog* **4**, e1000113.
4. Prusiner, S. B. (1998). Prions. *Proc Natl Acad Sci USA* **95**, 13363–13383.
5. Collinge, J. (2001). Prion diseases of humans and animals: their causes and molecular basis. *Annu Rev Neurosci* **24**, 519–550.

6. Weissmann, C., Enari, M., Klohn, P. C., Rossi, D. & Flechsig, E. (2002). Transmission of prions. *Proc Natl Acad Sci USA* **99**, 16378–16383.

7. Moore, R. A., Vorberg, I. & Priola, S. A. (2005). Species barriers in prion diseases – brief review. *Arch Virol* **Suppl 19**, 187–202.

8. Collinge, J., Sidle, K. C., Meads, J., Ironside, J. & Hill, A. F. (1996). Molecular analysis of prion strain variation and the aetiology of 'new variant' CJD. *Nature* **383**, 685–690.

9. Bruce, M. E., Will, R. G., Ironside, J. W., McConnell, I., Drummond, D., Suttie, A., McCardle, L., Chree, A., Hope, J., Birkett, C., Cousens, S., Fraser, H. & Bostock, C. J. (1997). Transmissions to mice indicate that 'new variant' CJD is caused by the BSE agent. *Nature* **389**, 498–501.

10. Hill, A. F., Desbruslais, M., Joiner, S., Sidle, K. C., Gowland, I., Collinge, J., Doey, L. J. & Lantos, P. (1997). The same prion strain causes vCJD and BSE. *Nature* **389**, 448–450, 526.

11. Collinge, J. (1999). Variant Creutzfeldt-Jakob disease. *Lancet* **354**, 317–323.

12. Westaway, D., Goodman, P. A., Mirenda, C. A., McKinley, M. P., Carlson, G. A. & Prusiner, S. B. (1987). Distinct prion proteins in short and long scrapie incubation period mice. *Cell* **51**, 651–662.

13. Hill, A. F. & Collinge, J. (2002). Species-barrier-independent prion replication in apparently resistant species. *Apmis* **110**, 44–53.

14. Riek, R., Hornemann, S., Wider, G., Billeter, M., Glockshuber, R. & Wüthrich, K. (1996). NMR structure of the mouse prion protein domain PrP(121–231). *Nature* **382**, 180–182.

15. James, T. L., Liu, H., Ulyanov, N. B., Farr-Jones, S., Zhang, H., Donne, D. G., Kaneko, K., Groth, D., Mehlhorn, I., Prusiner, S. B. & Cohen, F. E. (1997). Solution structure of a 142-residue recombinant prion protein corresponding to the infectious fragment of the scrapie isoform. *Proc Natl Acad Sci USA* **94**, 10086–10091.
16. Liu, H., Farr-Jones, S., Ulyanov, N. B., Llinas, M., Marqusee, S., Groth, D., Cohen, F. E., Prusiner, S. B. & James, T. L. (1999). Solution structure of Syrian hamster prion protein rPrP(90–231). *Biochemistry* **38**, 5362–5377.
17. Zahn, R., Liu, A., Lührs, T., Riek, R., von Schroetter, C., López-García, F., Billeter, M., Calzolai, L., Wider, G. & Wüthrich, K. (2000). NMR solution structure of the human prion protein. *Proc Natl Acad Sci USA* **97**, 145–150.
18. López-García, F., Zahn, R., Riek, R. & Wüthrich, K. (2000). NMR structure of the bovine prion protein. *Proc Natl Acad Sci USA* **97**, 8334–8339.
19. Hornemann, S., Schorn, C. & Wüthrich, K. (2004). NMR structure of the bovine prion protein isolated from healthy calf brains. *EMBO Rep* **5**, 1159–1164.
20. Gossert, A. D., Bonjour, S., Lysek, D. A., Fiorito, F. & Wüthrich, K. (2005). Prion protein NMR structures of elk and of mouse/elk hybrids. *Proc Natl Acad Sci USA* **102**, 646–650.
21. Lysek, D. A., Schorn, C., Nivon, L. G., Esteve-Moya, V., Christen, B., Calzolai, L., von Schroetter, C., Fiorito, F., Herrmann, T., Güntert, P. & Wüthrich, K. (2005). Prion protein NMR structures of cats, dogs, pigs, and sheep. *Proc Natl Acad Sci USA* **102**, 640–645.
22. Lysek, D. A. & Wüthrich, K. (2004). Prion protein interaction with the C-terminal SH3 domain of Grb2 studied using NMR and optical spectroscopy. *Biochemistry* **43**, 10393–10399.

23. Wopfner, F., Weidenhofer, G., Schneider, R., von Brunn, A., Gilch, S., Schwarz, T. F., Werner, T. & Schätzl, H. M. (1999). Analysis of 27 mammalian and 9 avian PrPs reveals high conservation of flexible regions of the prion protein. *J Mol Biol* **289**, 1163–1178.

24. van Rheede, T., Smolenaars, M. M., Madsen, O. & de Jong, W. W. (2003). Molecular evolution of the mammalian prion protein. *Mol Biol Evol* **20**, 111–121.

25. Morrissey, M. P. & Shakhnovich, E. I. (1999). Evidence for the role of PrP^{C} helix 1 in the hydrophilic seeding of prion aggregates. *Proc Natl Acad Sci USA* **96**, 11293–11298.

26. Priola, S. A., Chabry, J. & Chan, K. (2001). Efficient conversion of normal prion protein (PrP) by abnormal hamster PrP is determined by homology at amino acid residue 155. *J Virol* **75**, 4673–4680.

27. Gorfe, A. A. & Caflisch, A. (2007). Ser170 controls the conformational multiplicity of the loop 166–175 in prion proteins: implication for conversion and species barrier. *Faseb J* **21**, 3279–3287.

28. Telling, G. C., Scott, M., Mastrianni, J., Gabizon, R., Torchia, M., Cohen, F. E., DeArmond, S. J. & Prusiner, S. B. (1995). Prion propagation in mice expressing human and chimeric PrP transgenes implicates the interaction of cellular PrP with another protein. *Cell* **83**, 79–90.

29. Kaneko, K., Zulianello, L., Scott, M., Cooper, C. M., Wallace, A. C., James, T. L., Cohen, F. E. & Prusiner, S. B. (1997). Evidence for protein X binding to a discontinuous epitope on the cellular prion protein during scrapie prion propagation. *Proc Natl Acad Sci USA* **94**, 10069–10074.

30. Sigurdson, C. J. & Aguzzi, A. (2007). Chronic wasting disease. *Biochim Biophys Acta* **1772**, 610–618.

31. Cartoni, C., Schinina, M. E., Maras, B., Nonno, R., Vaccari, G., Di Baria, M. A., Conte, M., Liu, Q. G., Lu, M., Cardone, F., Windl, O., Pocchiari, M. & Agrimi, U. (2005). Identification of the pathological prion protein allotypes in scrapie-infected heterozygous bank voles (*Clethrionomys glareolus*) by high-performance liquid chromatography-mass spectrometry. *J Chromatogr A* **1081**, 122–126.

32. Billeter, M., Kline, A. D., Braun, W., Huber, R. & Wüthrich, K. (1989). Comparison of the high-resolution structures of the alpha-amylase inhibitor tendamistat determined by nuclear magnetic resonance in solution and by X-ray diffraction in single crystals. *J Mol Biol* **206**, 677–687.

33. Bax, A. & Grzesiek, S. (1993). Methodological advances in protein NMR. *Acc Chem Res* **26**, 131–138.

34. Dayie, K. T. & Wagner, G. (1994). Relaxation-rate measurements for 15N-1H groups with pulsed-field gradients and preservation of coherence pathways. *J Magn Reson A* **111**, 121–126.

35. Renner, C., Schleicher, M., Moroder, L. & Holak, T. A. (2002). Practical aspects of the 2D ^{15}N-{^{1}H}-NOE experiment. *J Biomol NMR* **23**, 23–33.

36. Keller, R. (2004). *The Computer-aided Resonance Assignment Tutorial CARA*. Cantina Verlag, Goldau, Switzerland.

37. Herrmann, T., Güntert, P. & Wüthrich, K. (2002). Protein NMR structure determination with automated NOE-identification in the NOESY spectra using the new software ATNOS. *J Biomol NMR* **24**, 171–189.

38. Herrmann, T., Güntert, P. & Wüthrich, K. (2002). Protein NMR structure determination with automated NOE assignment using the new software CANDID and the torsion angle dynamics algorithm DYANA. *J Mol Biol* **319**, 209–227.

39. Güntert, P., Mumenthaler, C. & Wüthrich, K. (1997). Torsion angle dynamics for NMR structure calculation with the new program DYANA. *J Mol Biol* **273**, 283–298.

40. Luginbühl, P., Güntert, P., Billeter, M. & Wüthrich, K. (1996). The new program OPAL for molecular dynamics simulations and energy refinements of biological macromolecules. *J Biomol NMR* **8**, 136–146.

41. Cornell, W. D., Cieplak, P., Bayly, C. I., Gould, I. R., Merz, K. M., Jr., Ferguson, D. M., Spellmeyer, D. C., Fox, T., Caldwell, J. W. & Kollman, P. A. (1995). A second generation force field for the simulation of proteins, nucleic acids, and organic molecules. *J Am Chem Soc* **117**, 5179–5197.

42. Koradi, R., Billeter, M. & Wüthrich, K. (1996). MOLMOL: a program for display and analysis of macromolecular structures. *J Mol Graph* **14**, 51–55.

43. Kabsch, W. & Sander, C. (1983). Dictionary of protein secondary structure: pattern recognition of hydrogen-bonded and geometrical features. *Biopolymers* **22**, 2577–2637.

44. Morris, A. L., MacArthur, M. W., Hutchinson, E. G. & Thornton, J. M. (1992). Stereochemical quality of protein structure coordinates. *Proteins* **12**, 345–364.

45. Schätzl, H. M., Da Costa, M., Taylor, L., Cohen, F. E. & Prusiner, S. B. (1995). Prion protein gene variation among primates. J Mol Biol 245, 362-374.

Figure captions

Figure 1

Amino acid sequence comparison of the C-terminal globular domain, spanning residues 121–231, of bank vole PrP (bvPrP, *Clethrionomys glareolus*, GenBank: AAL57231) with mouse PrP (mPrP, *Mus musculus*, GenBank:AAA39997), Syrian hamster PrP (shPrP, *Mesocricetus auratus*, GenBank:AAA37091), human PrP (hPrP, *Homo sapiens*, GenBank: AAA60182) and elk PrP (ePrP, *Cervus elaphus elaphus*, GenBank: AAU93885). The numeration of bvPrP and the locations of the regular secondary structures in bvPrP are indicated at the top. The complete sequence of bank vole PrP is given. For the other species, only amino acids that are different from bvPrP are indicated, with dots indicating the presence of identical amino acids, and dashes indicating deletions.

The mouse PrP variant mPrP[S170N](121–231) was generated from mPrP(121–231) by using the QuikChange® site-directed mutagenesis kit (Stratagene) according to the manufacturer's instructions, with the two primers 5'–CCA GTG GAT CAG TAC AAC AAC CAG AAC ACC–3' and 5'–GGT GTT CTG GTT GTT GTA CTG ATC CAC TGG–3'. As bvPrP(121–231) differs from mPrP(121–231) by only four amino acid substitutions (Y155N, S170N, D227E, R230S), its sequence was generated by three subsequent mutagenesis steps, starting from the plasmid encoding mPrP[S170N](121–231). The primers 5'–CGT GAA AAC ATG AAC CGC TAC CCT A–3' and 5'–T AGG GTA GCG GTT CAT GTT TTC ACG–3' were used for the mutagenesis Y155N, 5'–G GCC TAT TAC GAA GGG CGT CGT TCC–3' and 5'–GGA ACG ACG CCC TTC GTA ATA GGC C–3' for D227E, and 5'–GCC TAT TAC GAA GGG CGT AGC TCC TAG TAA GAA TTC GAA GCT

TGA–3' and 5'–TCA AGC TTC GAA TTC TTA TCA GGA ACT ACG CCC TTC GTA ATA GGC–3' for R230S.

Figure 2

Stereo views showing the residues 125–228 in the NMR structure of bvPrP(121–231). (A) Superposition of the 20 energy-minimized conformers used to represent the NMR structure. The N-terminal amino acid position 125 and sequence locations of the beginning and the end of the three α-helices are indicated. α-helices are highlighted in blue, β-strands are green, and the disulfide bond between residues 179 and 214 is orange. (B) All-heavy-atom presentation of the energy-minimized conformer with the lowest DYANA target function value. The backbone is represented by a grey spline function through the C^{α} positions. The side-chains are colored according to their global heavy atom displacements, D[32]: cyan, $D \leq 0.6$ Å; yellow, 0.6 Å $< D \leq 1.2$ Å; red, $D > 1.2$ Å.

Figure 3

Pairwise superpositions of the polypeptide segments 125–228 in the NMR structures of prion proteins that are related to the PrPs of three laboratory animals that are widely used in prion research. (A) bvPrP(121–231) (grey) and mPrP(121–231) (yellow). The radius of the cylindrical rods representing the polypeptide backbone is proportional to the mean global backbone displacement among the 20 energy-minimized conformers used to represent the NMR structures. For the residues of bvPrP(121–231) which differ from mPrP(121–231), red stick diagrams of the bundle of 20 conformers in Figure 2A are shown and identified with red lettering. (B) bvPrP(121–231) (grey) and shPrP(121–231) (green). Same presentation as (A), with the variable side chains in green. (C) bvPrP(121–231)

(grey) and mPrP[S170N](121-231) (blue). Same presentation as (A), with variable side chains in blue.

Figure 4

2D [^{15}N,^{1}H]-HSQC spectra recorded at a ^{1}H frequency of 500 MHz and T = 20°C. (A) mPrP(121–231). (B) bvPrP(121–231). (C) mPrP[S170N](121–231). The peaks corresponding to residues 166−175 are highlighted, with blue circles identifying peaks that are present in all three spectra, and red circles around peaks that were not observed in mPrP(121−231). The Asn170 and Phe175 peaks of bvPrP(121−231) and mPrP[S170N](121−231) are broadened when compared to the other peaks in the same spectra, and therefore only weak contours are seen.

Table caption

Table 1

Input for the structure calculations and characterization of the energy-minimized NMR structures of bvPrP(121–231) and mPrP[S170N](121–231).

[a] Except for the two top entries, the average value for the 20 energy-minimized conformers with the lowest residual DYANA target function values and the standard deviation among them are given.

[b] NMR experiments were performed at 20°C with uniformly ^{15}N- or ^{13}C,^{15}N-labeled protein samples of bvPrP(121–231), and at 25°C with mPrP[S170N](121–231). Both proteins had been expressed in *E. coli* and purified following standard procedures.[17,22] The NMR samples contained protein concentrations of 0.4–1.0 mM in 10 mM [d_4]-sodium acetate buffer, pH 4.5, 90% H_2O/10% D_2O. Standard triple resonance NMR experiments[33] were recorded on a Bruker DRX 500 spectrometer equipped with a triply tuneable cryogenic probehead to obtain sequence-specific resonance assignments. Side-chain assignments were obtained with 3D ^{15}N-resolved [^{1}H,^{1}H]-TOCSY and 3D HCCH-TOCSY spectra measured on a Bruker DRX 600 spectromter equipped with a triple-resonance z-gradient probehead. Steady-state ^{15}N{^{1}H}-nuclear Overhauser enhancements (NOEs) were measured with recovery delays and proton saturation periods of 2 and 3 sec, respectively, and for the reference experiment we used a 5 sec recovery period.[34,35] The program CARA[36] was used for the spectral analysis.

3D ^{15}N-resolved [^{1}H,^{1}H]-NOESY spectra were recorded at a ^{1}H frequency of 900 MHz for bvPrP(121–231) and of 750 MHz for mPrP[S170N](121–231). For both proteins, two 3D ^{13}C-resolved [^{1}H,^{1}H]-NOESY spectra were collected at 750 MHz, with the ^{13}C carrier frequency either in the aliphatic or the aromatic region. All NOESY data sets were measured with a mixing time of 60 ms. Automatic peak picking and NOE assignment was

performed using the standalone ATNOS/CANDID program package.[37,38] The final cycle of the structure calculation with DYANA[39] was started with 100 randomized conformers; the 20 conformers with the lowest residual target function values were energy-minimized in a water shell with the program OPALp[40] using the AMBER force field.[41] The program MOLMOL[42] was used to analyze the results of the structure calculations and to prepare the drawings of the structures. Regular secondary structure boundaries were determined with MOLMOL, using the method of Kabsch and Sander.[43]

[c] bb indicates the backbone atoms N, C^{α}, C'; ha stands for "all heavy atoms". The numbers in parentheses indicate the residues for which the rmsd values were calculated.

[d] As determined by PROCHECK.[44]

Figure 1

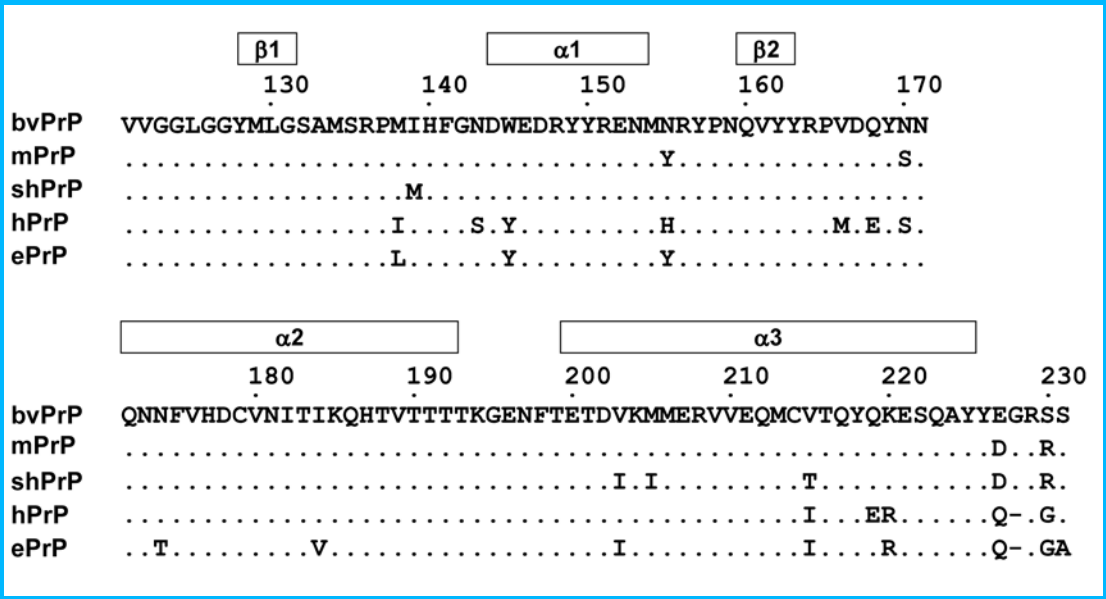
β1
α1
β2
130
140
150
160
170
bvPrP VVGGLGGYMLGSAMSRPMIHFGNDWEDRYYRENMNRYPNQVYYRPVDQYNN
mPrP .....Y.....S.
shPrP .....M.....
hPrP .....I....S.Y.....H.....M.E.S.
ePrP .....L.....Y.....Y.....
α2
α3
180
190
200
210
220
230
bvPrP QNNFVHDCVNITIKQHTVTTTTKGENFTETDVKMMERVVEQMCVTQYQKESQAYYEGRSS
mPrP .....D..R.
shPrP .....I.I.....T.....D..R.
hPrP .....I...ER.....Q-.G.
ePrP ..T.....V.....I.....I....R.....Q-.GA

Figure 2

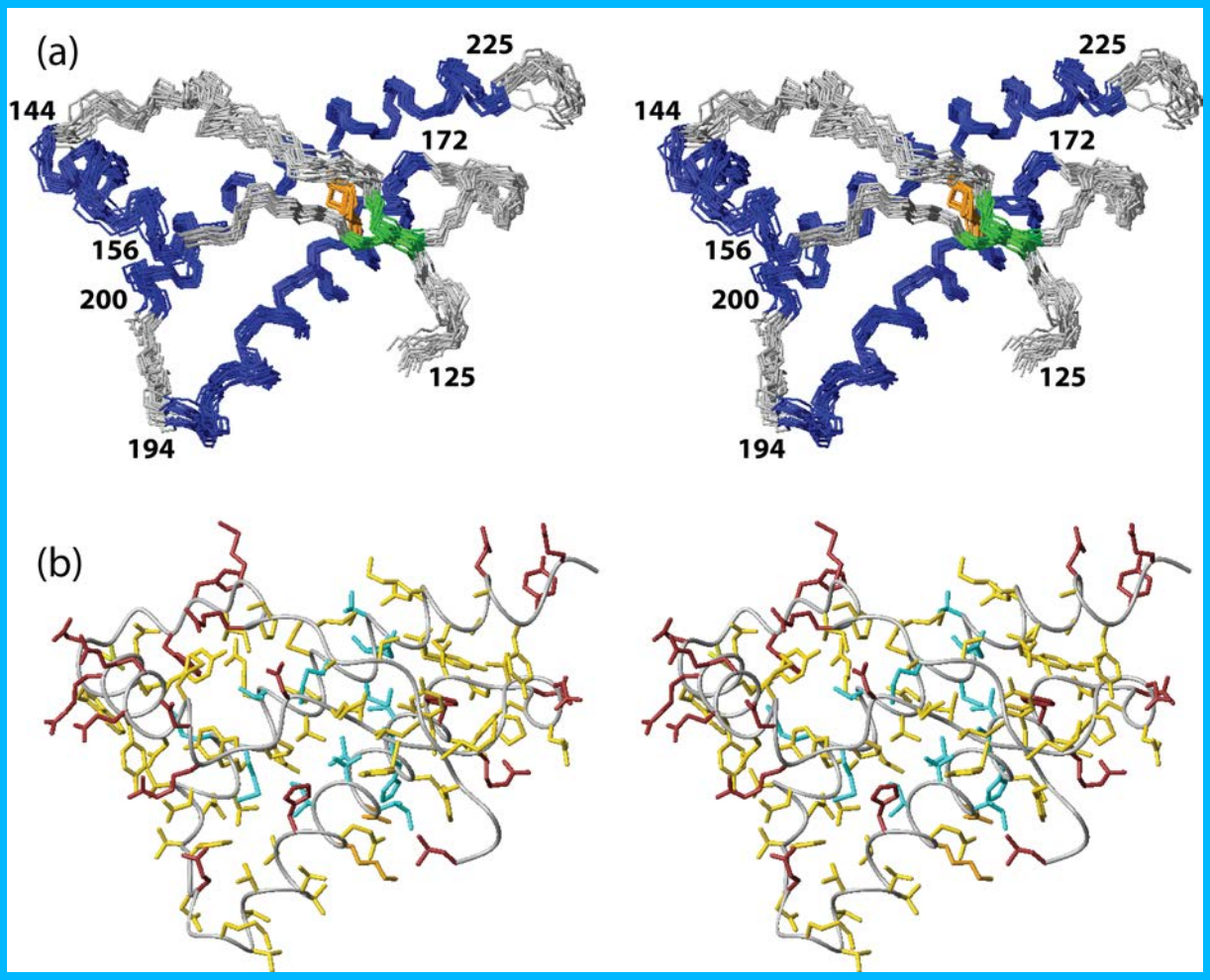

Figure 3

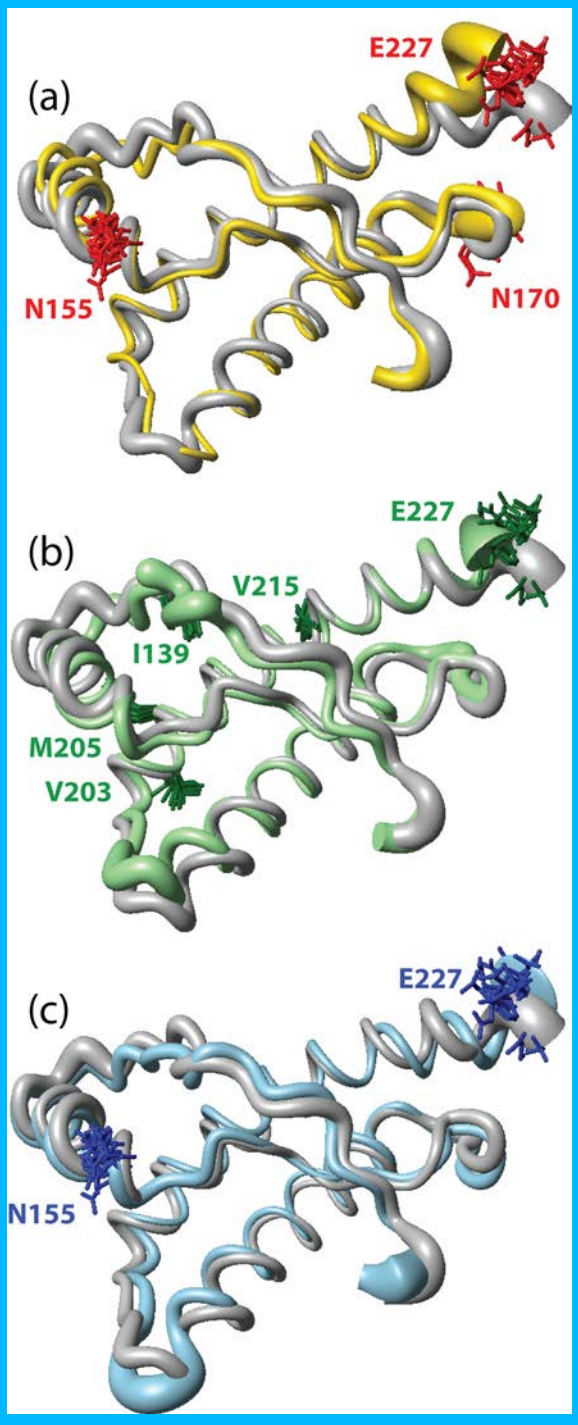

Figure 4

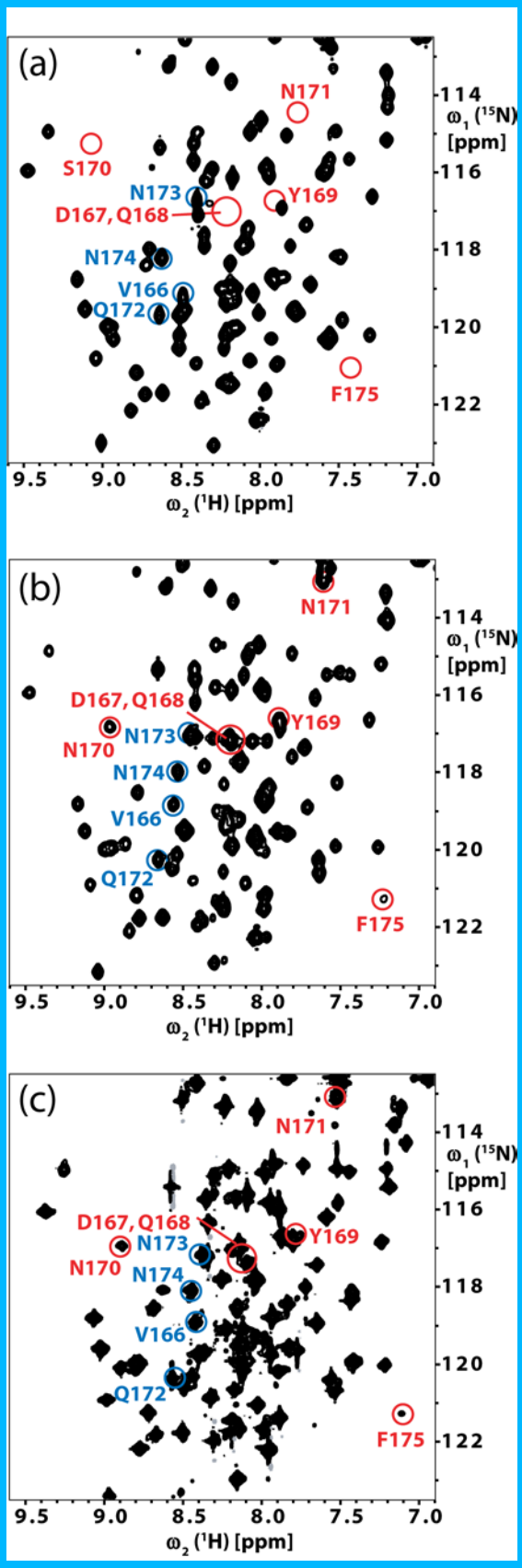
(a)
N171
S170
N173
Y169
D167, Q168
N174
V166
Q172
F175
114
116
118
120
122
ω1 (15N) [ppm]
9.5
9.0
8.5
8.0
7.5
7.0
ω2 (1H) [ppm]
(b)
N171
D167, Q168
Y169
N173
N170
N174
V166
Q172
F175
(c)
N171
D167, Q168
Y169
N173
N170
N174
V166
Q172
F175

Table 1

	bvPr(121–231)[a]	**mPrP[S170N](121–231)[a]**
NOE upper distance limits[b]	1694	1567
Dihedral angle constraints	114	116
Residual target function value (Å^2)	1.15 ± 0.40	1.39 ± 0.29
Residual distance constraint violations		
Number > 0.1 Å	25 ± 4	25 ± 4
Maximum (Å)	0.14 ± 0.01	0.14 ± 0.01
Residual dihedral angle constraint violations		
Number > 2.0 deg	0 ± 0	0 ± 0
Maximum (deg)	0.97 ± 1.32	1.35 ± 0.98
Amber energies (kcal/mol)		
Total	–4873 ± 66	–4893 ± 114
Van der Waals	–329 ± 14	–337 ± 17
Electrostatic	–5467 ± 65	–5482 ± 107
rmsd to the mean coordinates (Å)[c]		
bb (125–226)	0.68 ± 0.08	0.68 ± 0.10
ha (125–226)	1.10 ± 0.10	1.11 ± 0.09
Ramachandran plot statistics[d]		
Most favored regions (%)	85	85
Additional allowed regions (%)	14	13
Generously allowed regions (%)	1	2
Disallowed regions (%)	0	0